Graph-Structure Based Multi-Granular Belief Fusion for Human Activity Recognition

Yilin Dong, Xinde Li, *Senior Member, IEEE,* Jean Dezert, Rigui Zhou, Kezhu Zuo and Shuzhi Sam Ge, *Fellow, IEEE*

***Abstract*—The Belief Functions (BFs) introduced by Shafer in the mid of 1970s are widely applied in information fusion to model epistemic uncertainty and to reason about uncertainty. Their success in applications is however limited because of their high computational complexity in the fusion process, especially when the number of focal elements is large. To reduce the complexity of reasoning with BFs, we can envisage as a first method to reduce the number of focal elements involved in the fusion process to convert the original Basic Belief Assignments (BBAs) into simpler ones, or as a second method to use a simple rule of combination with potentially a loss of the specificity and pertinence of the fusion result, or to apply both methods jointly. In this paper, we focus on the first method and propose a new BBA granulation method inspired by the community clustering of nodes in graph networks. This paper studies a novel efficient Multi-Granular Belief Fusion method (MGBF). Specifically, focal elements are regarded as nodes in the graph structure, and the distance between nodes will be used to discover the local community relationship of focal elements. Afterwards, the nodes belonging to the decision-making community are specially selected, and then the derived multi-granular sources of evidence can be efficiently combined. To evaluate the effectiveness of the proposed graph-based MGBF, we further apply this new approach to combine the outputs of Convolutional Neural Networks+Attention (CNN+Attention) in the human activity recognition problem. The experimental results obtained with real datasets prove the potential interest and feasibility of our proposed strategy with respect to classical BF fusion methods.**

***Index Terms*—Belief Functions, Basic Belief Assignment, Graph Networks, Multi-Granular Fusion, Human Activity Recognition.**

I. Introduction

A. Background and Research Motivation

This work was supported in part by the National Natural Science Foundation of China under Grant 62103258, 62233003 and 62073072, and in part by the Key Projects of Key R&D Program of Jiangsu Province under Grant BE2020006 and Grant BE2020006-1 and in part by Shenzhen Natural Science Foundation under Grant JCYJ20210324132202005 and JCYJ20220818101206014. (*Corresponding authors:Xinde Li; Rigui Zhou.*)

Yilin Dong is with College of Information Engineering, Shanghai Maritime University. Email:yldong@shmtu.edu.cn.

Xinde Li is with Key Laboratory of Measurement and Control of CSE, School of Automation, Southeast University. Email:xindeli@seu.edu.cn.

Jean Dezert is with The French Aerospace Lab, ONERA, DTIS, F-91123 Palaiseau, France. Email:jean.dezert@onera.fr.

Rigui Zhou is with College of Information Engineering, Shanghai Maritime University, Shanghai, China. Email:rgzhou@shmtu.edu.cn.

Kezhu Zuo is with Key Laboratory of Measurement and Control of CSE, School of Automation, Southeast University. Email:18640168697@163.com.

Shuzhi Sam Ge is with the Social Robotics Laboratory, Department of Electrical and Computer Engineering, Interactive Digital Media Institute, National University of Singapore, Singapore. (Email:samge@nus.edu.sg).

THE Belief Functions (BFs) have introduced in.1976 by Shafer in his mathematical Theory of Evidence, also known as Dempster-Shafer Theory (DST) for reasoning about epistemic uncertainty. They have been widely used in fault diagnosis [1, 2], activity recognition [3–6], indoor location [7, 8], and other uncertainty modeling and reasoning application areas [9, 10]. However, BFs have been criticized for their inherent complexity [11], especially in the worse case analysis. A widely discussed drawback is the exponential computational complexity of most existing rules of combination of sources of evidence, especially when the cardinality of the Frame of Discernment (FoD) and the number of focal elements of the Basic Belief Assignment (BBA) become large. Currently, the high computational burden restricts the practical application of BFs [12–14]. To overcome this serious problem, many scholars have proposed various BBA approximation methods, which mainly rely on three principles: the first one is to reduce the dimension of BBAs according to the belief masses of focal elements: those focal elements with smaller masses are regarded as unimportant ones and should be removed first. The representative methods include $k-l-x$ [15], Summarization [16] and $D1$ [17]. The second approximation strategy is mainly implemented based on the cardinality of the focal element itself. That is, the focal element with a larger cardinality is removed to reduce the computational complexity in the fusion process. The k-additive approximation [18] followed this kind of simplification approach. The third type of approximation method is to jointly use the belief masses and the cardinality of the focal element to determine which focal element should be removed first. Representative works include internal and external approximations [19]. The ultimate goal of these BBA approximation strategies is to obtain a simpler BBA by removing the redundant focal elements according to specific chosen criteria. Although all the aforementioned approaches are reasonable and meaningful to a certain extent, they still have their limitations, which mainly lie in three aspects:

- Although the distance metrics between focal elements have been proposed, the degradation of original BBA in the process of BBA approximation is still unavoidable, which in turn affects the performance of the decision-level fusion;
- As far as we know, only few theoretical approximation methods can intuitively observe the affinities between focal elements through visualization. The visualization of the relationship between nodes is one of the advantages

of graph networks;
- All existing BBA approximation methods developed so far focus on the theoretical level, and there are few works done to verify the effectiveness of the approximate fusion methods in practical applications. Besides, we also need to consider whether the classical step-by-step approximation for changing the original BBA little by little is necessary for practical application.

Regarding the first and second aspects, the inherent relationship between focal elements needs to be further discussed and analyzed to avoid degradation as much as possible. However, the classical approximation methods mentioned above focused on their discussions on evaluating the local characteristics (such as uncertainty or entropy) of the single focal element in the evidence. From a global perspective, it is extremely important to analyze the proximity and structural information between focal elements. At present, more and more scholars study the relationship between focal elements in the sources of evidence. For example, Chen et al. [20] proposed a novel Probabilistic Transformation (PT) method based on an ordered visibility graph. In this method, all focal elements were first sorted based on the non-effective belief entropy [21], and then a weighted network structure was constructed to obtain the Bayesian BBA. In this paper, to achieve the simplification of the BBA, we discuss the aggregation of focal elements under the condition of graph network structure, which is quite different from the method proposed in [20]. Regarding the third aspect, very few works have been done that do not attract much attention to provide new interest for the applications of BFs. In fact, there are some related works that combine graph structure-based visualization with BFs, but the focus of the research done is fundamentally different from the issues discussed in this paper. For example, Zhao et al. [22] characterized evidence sources as nodes in a graph network to discuss the weighted fusion of high-conflict sources of evidence; Xiong et al. [23] also realized the weighted combination of BBAs with the help of the complex networks. These two recent works aim to deal with the classical combination problems when sources of evidence are in highly conflict with each other. In this paper, the original motivation for using graph structure visualization and convenience is to reveal the structural relationship information between focal elements. This necessary step is also a preparation for the subsequent community detection and multi-granular mapping between focal elements. It is worth noting that the Multi-Granular Belief Fusion (MGBF) proposed in this paper has a different emphasis from the well-known BBA approximation. MGBF in this paper includes two main steps: 1. This strategy first focuses on the agglomeration of fine focal elements into larger or coarse granular ones to find the inherent communities hidden in focal elements; 2. Then, the specific focal elements will be selected in the decision-making community, which aims to preserve the decision information in the original BBA as much as possible; traditional BBA approximation aims to obtain the specific simpler BBA, which is intentionally overall similar or closer but not exactly equal to the original BBA.

B. Challenges

To achieve the efficient graph-based multi-granular belief fusion, three main issues need to be addressed:

- How to determine the distance degree between focal elements? This value mainly determines the quality of community discovery in focal elements;
- How to implement aggregation for focal elements in the same community, and how to calculate the belief masses of the derived multi-granular focal elements in the decision-making community?
- How to effectively use the proposed multi-granular fusion strategy in the practical application? This novel fusion strategy aims to reduce the computational complexity of the fusion process to ensure recognition accuracy.

C. Main Contributions

To solve these three aforementioned problems, we propose a multi-granular belief fusion method based on graph structure for BBA granulation. Also, we apply our proposed approach to deal with Human Activity Recognition (HAR) problem. In this paper, we first measure the dissimilarity between focal elements and thus generate the adjacency matrix between focal elements. Based on this matrix, we can discover the potential graph-based communities in focal elements. Communities are often defined in terms of the partition of the set of nodes, where each node is put into one and only one community. Communities are used to describe the potential relationship between focal elements, which comes from the graph theory [24]. This might happen in a human activity problem where each focal element represents an activity, and the communities represent the different groups of activities: one community for static activities, another community for dynamic activities. In this article, communities can be detected in a set of focal elements, and two types of communities will be particularly generated: the decision-making community and the supporting community. Among them, the decision-making community mainly includes the focal elements that play a significant role in the final decision-making results, such as those with high belief masses, while the supporting community mainly consists of the focal elements that play a minor role in the final decision making. Then, the decision-making community is divided into the representative fine-grained focal elements and the belief masses of these core focal elements can be updated with the help of the remaining focal elements in the supporting community. Finally, the simpler multi-granular sources of evidence can be combined by using the classical Proportional Conflict Redistribution rule #6 (PCR6) rule of combination developed originally in Dezert-Smarandache Theory (DSmT) [25]. The main contributions of this paper are summarized as follows:

- This work proposes for the first time a multi-granular belief fusion to tackle the problems of BBA granulation. With this new approach, the potential relationships between focal elements can be detected and visualized based on the graph structure. This allows us to easily identify the focal elements belonging to the same com-

munity. This multi-granular mapping can make efficient granulation of the original BBAs into fine-grained ones;
- We evaluate the effectiveness of this MGBF approach in the HAR problems. In this application, the proposed fusion method is adopted to fuse the outputs of end-to-end CNN+Attention networks. Besides, extensive experiments of comparisons are conducted to show the efficiency of the proposed method.

The rest of this paper is organized as follows. In section II, the basics of BFs and graph networks are presented. Section III describes the proposed multi-granular belief fusion method for BBA granulation. The human activity recognition problems and the related experimental results are given in detail in Section IV. Finally, the article concludes and gives several future research directions in the last section.

II. Preliminaries

A. Basics of BFs

In BFs, the concept of FoD represents a set of exhaustive and exclusive elements which is denoted as $\Theta \triangleq \{\theta_1, \ldots, \theta_n\}$ ($n \geq 2$). The power set of Θ, which is the set of all subsets of Θ (including the empty set $\emptyset$, and Θ itself), is denoted 2^Θ because its cardinality is exactly equal to $2^{|\Theta|}$. A Basic Belief Assignment (BBA) $m(\cdot)$ is defined by the mapping: $2^\Theta \mapsto [0,1]$, verifying $m(\emptyset) = 0$ and $\sum_{X \in 2^\Theta} m(X) = 1$. A subset X of Θ is called a focal element of a BBA $m(\cdot)$ if and only if $m(X) > 0$. Besides, the set of focal elements of a BBA $m(\cdot)$ is denoted $\mathcal{F}(m)$ and $|\mathcal{F}(m)|$ represents the number of focal elements of $m(\cdot)$. A BBA is bayesian if all its focal elements are singletons of the power set of Θ, otherwise it is referred as a non-bayesian BBA. A source of evidence totally ignorant is represented by the so-called vacuous BBA $m_{va}(\cdot)$ for which $m_{va}(X) = 0$ for all $X \subset \Theta$ and $m_{va}(\Theta) = 1$. The belief and plausibility functions are respectively defined for any subset $A \in 2^\Theta$ by[1] - see [26]

$$Bel(A) \triangleq \sum_{X \in 2^\Theta | X \subseteq A} m(X) \tag{1}$$

and

$$Pl(A) \triangleq \sum_{X \in 2^\Theta | X \cap A \neq \emptyset} m(X) \tag{2}$$

In order to combine two distinct sources of evidence, the classical Dempster-Shafer rule (DS) in [26] was proposed and defined by $m_{DS}(\emptyset) = 0$ and $\forall A \in 2^\Theta \setminus \{\emptyset\}$:

$$m_{DS}(A) = \frac{\sum_{X_1, X_2 \in 2^\Theta | X_1 \cap X_2 = A} m_1(X_1) m_2(X_2)}{1 - \sum_{X_1, X_2 \in 2^\Theta | X_1 \cap X_2 = \emptyset} m_1(X_1) m_2(X_2)}. \tag{3}$$

To palliate DS rule drawbacks (see discussions in [27]), the new Proportional Conflict Redistribution rule #6 (PCR6) was defined [25] for combining two BBAs by: $m_{PCR6}(\emptyset) = 0$ and $\forall A \in 2^\Theta \setminus \{\emptyset\}$:

$$m_{PCR6}(A) = m_{12}(A) + \sum_{X \in 2^\Theta | X \cap A = \emptyset} \left[\frac{m_1(A)^2 m_2(X)}{m_1(A) + m_2(X)} + \frac{m_2(A)^2 m_1(X)}{m_2(A) + m_1(X)}\right]. \tag{4}$$

where $m_{12}(A) = \sum_{X_1, X_2 \in 2^\Theta | X_1 \cap X_2 = A} m_1(X_1) m_2(X_2)$ is the conjunctive rule of the two BBAs $m_1(.)$ and $m_2(.)$, and where all denominators in (4) are different from zero. If a denominator is zero, that fraction is discarded. The general PCR6 formula for combining more than two BBAs altogether is given in [25], Vol. 3.

B. Basics of Graph Networks

Generally, a graph is a two-tuple composed of a set of points $V = \{v_i\}$ and a set of unordered pairs of elements in $E = \{e_k\}$, denoted as $G = (V, E)$. The elements v_i in V is called a node, and then element e_k in E is called an edge [28, 29]. We can use $e_{ij} = 1$ to represent node i is associated with node j. If $e_{ij} = 0$, it means node i is unrelated to node j.

In a graph network, the adjacency matrix can represent the adjacency between nodes. Considering a graph $G = (V, E)$, the adjacency matrix of G having n nodes is an $n \times n$ matrix with the following properties:

- If there is an edge between node i and node j, the element A_{ij} in the matrix is 1, otherwise it is 0;
- For an undirected graph, the adjacency matrix is symmetric, and the main diagonal is zero.

III. Multi-granular belief fusion based on graph structure

Inspired by the interaction between nodes in graph networks, a novel graph-based multi-granular belief fusion method for BBA granulation is proposed. This novel approach can discover communities in original focal elements and then realize the multi-granular mapping within communities. Afterwards, the multi-granular fusion can be easily implemented in the multi-grained layer to reduce the computational complexity of the original high-dimensional evidence fusion.

A. The Framework of Multi-Granular Belief Fusion

Fig.1 shows the framework of the proposed efficient multi-granular belief fusion method. The main steps of MGBF are:

- Step 1: the distance between focal elements is measured to construct the dissimilarity and adjacency matrix. Then, the relationship between focal elements can be visualized;
- Step 2: the inner community can be detected among focal elements, and those specific elements in the decision-making community are selected to realize the multi-granular mapping;
- Step 3: the derived multi-granular sources of evidence can be efficiently fused based on the classical PCR6 rule.

[1]The symbol $\triangleq$ means *equal by definition.*

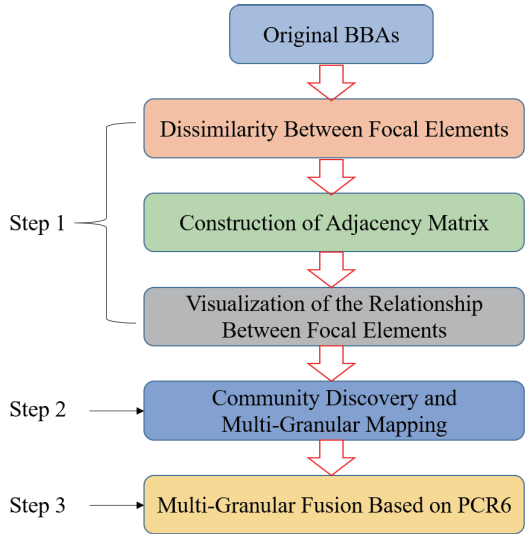

Fig. 1: **The Framework of Multi-Granular Belief Fusion for BBA Granulation.**

B. Construction of adjacency matrix and visualization

To complete the deletion of quasi-redundant focal elements in traditional BBA approximation, researchers have proposed several methods [11, 17, 19] based on some measures of dissimilarity of focal elements. In this paper, we go further and present the relationships of focal elements represented by graphs. Based on this type of representation, we can more easily identify and visualize the communities existing among focal elements, and then complete the multi-granular mapping of the fine-grained focal elements of the original sources of evidence. The distance between focal elements usually represents the dissimilarity between focal elements, which is of great significance for effective BBA granulation. Generally speaking, it should meet the characteristics of non-negativity and symmetry. Denœux proposed in [19] a method to evaluate the impact of the transfer of the masses of focal elements F_i and F_j to their union $F_i \cup F_j$ on Weighted Average of the Cardinalities of Focal Elements (WACFE) of $m(\cdot)$ defined[2] by $|m| = \sum_{F\in 2^\Theta} m(F)\cdot|F|$. This impact for any pair of focal elements F_i and F_j corresponds to an increase $\delta^m_\cup(F_i,F_j)$ of $|m|$ given by[3] (see [19])

$$\delta^m_\cup(F_i,F_j) \triangleq [m(F_i)+m(F_j)]|F_i\cup F_j| - m(F_i)|F_i| - m(F_j)|F_j| \quad (5)$$

where $m(\cdot)$ and $|\cdot|$ denote respectively the mass and cardinality of the focal element.

Example 1: suppose $\Theta=\{A,B,C\}$ and the non-bayesian BBA given by $m(A)=0.3$, $m(B)=0.1$, $m(C)=0.2$, $m(A\cup B)=0.1$ and $m(\Theta)=0.3$. Then one gets

$$\begin{aligned}|m| &= m(A\cdot)|A| + m(B)\cdot|B| + m(C)\cdot|C| \\ &\quad + m(A\cup B)\cdot|A\cup B| + m(\Theta)\cdot|\Theta| \\ &= 0.3\cdot 1 + 0.1\cdot 1 + 0.2\cdot 1 + 0.1\cdot 2 + 0.3\cdot 3 = 1.7\end{aligned}$$

If we modify this BBA by transferring the masses $m(A)=0.3$ and $m(B)=0.1$ to their union $m(A\cup B)$, we obtain the modified BBA $m'(\cdot)$ whose values are $m'(C)=m(C)=0.2$, $m'(A\cup B)=m(A\cup B)+m(A)+m(B)=0.5$ and $m'(\Theta)=m(\Theta)=0.3$, and the WACFE of the modified BBA $m'(\cdot)$ is

$$\begin{aligned}|m'| &= m'(C)\cdot|C| + m'(A\cup B)\cdot|A\cup B| + m'(\Theta)\cdot|\Theta| \\ &= 0.2\cdot 1 + 0.5\cdot 2 + 0.3\cdot 3 = 2.1\end{aligned}$$

This corresponds to an increase $|m'|-|m| = 2.1-1.7 = 0.4$ of the WACFE of m, which is given by (5). We can easily verify

$$\begin{aligned}\delta^m_\cup(A,B) &= [m(A)+m(B)]|A\cup B| - m(A)|A| - m(B)|B| \\ &= [0.3+0.1]\cdot 2 - 0.3\cdot 1 - 0.1\cdot 1 = 0.4\end{aligned}$$

According to Denœux [19], the quantity $\delta^m_\cup(F_i,F_j)$ defined in (5) measures the impact of replacing F_i and F_j by their union, and can therefore be interpreted somehow as a "distance" between these two focal elements F_i and F_j.

Based on Denœux idea, we can define an Impact Union-based matrix (IU matrix for short) $\mathbf{\Delta}(m)$ defined by

$$\mathbf{\Delta}(m) \triangleq [\delta^m_\cup(F_i,F_j), 0<i,j\leq|\mathcal{F}(m)|] \quad (6)$$

where $\delta^m_\cup(F_i,F_j)$ is the impact on WACFE of the original BBA $m(\cdot)$ when replacing F_i and F_j by their union, and where i and j are the indexes of the elements in $\mathcal{F}(m)$. Note that this IU matrix $\mathbf{\Delta}(m)$ is a $|\mathcal{F}(m)|\times|\mathcal{F}(m)|$ matrix. Note also that the IU matrix is symmetrical because $\delta^m_\cup(F_i,F_j) = \delta^m_\cup(F_j,F_i)$ for any index i and j. Also, the components of the main diagonal of the IU matrix $\mathbf{\Delta}(m)$ are all equal to zero because $\delta^m_\cup(F_i,F_i) = [m(F_i)+m(F_i)]\cdot|F_i\cup F_i| - m(F_i)\cdot|F_i| - m(F_i)\cdot|F_i| = 0$ since $|F_i\cup F_i| = |F_i|$.

Example 1 (continued): the rows and the columns of from 1 to $|\mathcal{F}(m)|=5$ correspond respectively to focal elements A, B, C, $A\cup B$, and $A\cup B\cup C\equiv\Theta$ in $\mathcal{F}(m)$, and in this example the IU matrix is equal to

$$\mathbf{\Delta}(m) = \begin{bmatrix} 0 & 0.4 & 0.5 & 0.3 & 0.6 \\ 0.4 & 0 & 0.3 & 0.1 & 0.2 \\ 0.5 & 0.3 & 0 & 0.5 & 0.4 \\ 0.3 & 0.1 & 0.5 & 0 & 0.1 \\ 0.6 & 0.2 & 0.4 & 0.1 & 0 \end{bmatrix}$$

The calculation of elements $\Delta_{ij}(m)$ of the IU matrix $\mathbf{\Delta}(m)$ is done according to (5). For instance, the component $\Delta_{14}(m)=0.3$ because from (5) we have

$$\begin{aligned}\Delta_{14}(m) &= \delta^m_\cup(A, A\cup B) \\ &= [m(A)+m(A\cup B)]\cdot|A\cup(A\cup B)| \\ &\quad - m(A)\cdot|A| - m(A\cup B)\cdot|A\cup B| \\ &= [0.3+0.1]\cdot 2 - 0.3\cdot 1 - 0.1\cdot 2 = 0.3\end{aligned}$$

We recall that the first element (corresponding to index value 1) and the forth element (corresponding to index value 4)

[2] In [19], the weighted average of the cardinalities of focal elements of $m(\cdot)$ is called the *generalized cardinality* of $m(\cdot)$.

[3] In $\delta^m_\cup$ the m notation in superscript refers explicitly to the BBA $m(\cdot)$ (and not to a numerical power exponent). This is because $\delta^m_\cup(F_i,F_j)$ depends on the values of masses of focal elements of the BBA $m(\cdot)$.

of $\mathcal{F}(m)$ are respectively A and $A \cup B$, and that is why $\Delta_{14}(m) = \delta^m_{\cup}(A, A \cup B)$.

For our BBA granulation purpose, we can always define an adjacency matrix, denoted by $\mathbf{AM}(m)$ from the calculation of IU matrix $\mathbf{\Delta}(m)$ based on some thresholding strategy for selecting the most impacting pairs of elements of the power set on the change of WACFE of the original BBA when transferring their mass to their union. The adjacency matrix $\mathbf{AM}(m) = [AM_{ij}(m)]$ is a $|\mathcal{F}(m)| \times |\mathcal{F}(m)|$ matrix whose the components are given by

$$AM_{ij}(m) = \begin{cases} 1, \text{ if } \delta^m_{\cup}(F_i, F_j) \geq \rho, \\ 0, \text{ if } \delta^m_{\cup}(F_i, F_j) < \rho. \end{cases} \tag{7}$$

where ρ is a chosen threshold value.

The choice of the threshold value ρ is one of the most critical steps in the traditional construction of graph structure. When the threshold ρ is small, there will exists many connections between nodes (i.e. focal elements of $m(\cdot)$) in the graph structure, which will generate the dense graph and thus increase the computational complexity of the subsequent fusion steps. Conversely, when the threshold ρ is large, it may connect some conflicting focal elements and transform the dense graph into a sparse graph. Therefore, whether the threshold ρ is too large or too small, it will affect the relationship between focal elements. Based on the obtained IU matrix $\mathbf{\Delta}(m)$, the adjacency matrix can always be constructed based on the selection of the threshold ρ, which is regarded as the basis of graph analysis.

Example 1 (continued): suppose we take to $\rho = 0.4$ as the threshold value for building the adjacency matrix $\mathbf{AM}(m)$. From IU matrix obtained for this example, we get

$$\mathbf{AM}(m) = \begin{bmatrix} 0 & 1 & 1 & 0 & 1 \\ 1 & 0 & 0 & 0 & 0 \\ 1 & 0 & 0 & 1 & 1 \\ 0 & 0 & 1 & 0 & 0 \\ 1 & 0 & 1 & 0 & 0 \end{bmatrix}$$

Generally speaking, an adjacency matrix is a mathematical representation of a graph, which will directly reflect the connection relationship between focal elements for making a BBA granulation.

To circumvent the problem of threshold selection, we propose in this work a method of construction of the adjacency matrix based on the maximum value of $\delta^m_{\cup}(F_i, F_j)$ of IU matrix (6). In our proposed method, a pair of focal elements with the largest $\delta^m_{\cup}(F_i, F_j)$ are found, and the corresponding value is denoted as 1 in the adjacency matrix. Meanwhile, the values of other components of the adjacency matrix are set to 0. Based on this very simple strategy, we can identify and mark the focal elements that play a decisive role in the source of evidence, aiming to pave the way for subsequent decision-making.

$$AM_{ij}(m) = \begin{cases} 1, \text{ if } \delta^m_{\cup}(F_i, F_j) = \max \mathbf{\Delta}(m), \\ 0, \text{ otherwise.} \end{cases} \tag{8}$$

Example 1 (continued): based on the simple adjacency matrix construction (8), we will get in this non-bayesian BBA example

$$\mathbf{AM}(m) = \begin{bmatrix} 0 & 0 & 0 & 0 & 1 \\ 0 & 0 & 0 & 0 & 0 \\ 0 & 0 & 0 & 0 & 0 \\ 0 & 0 & 0 & 0 & 0 \\ 1 & 0 & 0 & 0 & 0 \end{bmatrix}$$

Example 2: we consider here an other example with bayesian BBAs where the FoD is $\Theta = \{\theta_1, \theta_2, \theta_3, \theta_4, \theta_5, \theta_6\}$. Suppose we have two Bayesian BBAs given as in Table I.

TABLE I: Bayesian BBAs.

Focal elem.	$m_1(\cdot)$	$m_2(\cdot)$
θ_1	0.70	0.10
θ_2	0.10	0.10
θ_3	0.01	0.04
θ_4	0.05	0.15
θ_5	0.05	0.60
θ_6	0.09	0.01

Here, $\mathcal{F}(m_1) = \mathcal{F}(m_2) = \{\theta_1, \theta_2, \theta_3, \theta_4, \theta_5, \theta_6\}$ and $|\mathcal{F}(m)| = 6$. For these bayesian BBAs $m_1(\cdot)$ and $m_2(\cdot)$, the IU matrices are respectively equal to

$$\mathbf{\Delta}(m_1) = \begin{bmatrix} 0 & 0.80 & 0.71 & 0.75 & 0.75 & 0.79 \\ 0.80 & 0 & 0.11 & 0.15 & 0.15 & 0.19 \\ 0.71 & 0.11 & 0 & 0.06 & 0.06 & 0.1 \\ 0.75 & 0.15 & 0.06 & 0 & 0.10 & 0.14 \\ 0.75 & 0.15 & 0.06 & 0.10 & 0 & 0.14 \\ 0.79 & 0.19 & 0.10 & 0.14 & 0.14 & 0 \end{bmatrix}$$

$$\mathbf{\Delta}(m_2) = \begin{bmatrix} 0 & 0.2 & 0.14 & 0.25 & 0.70 & 0.11 \\ 0.20 & 0 & 0.14 & 0.25 & 0.70 & 0.11 \\ 0.14 & 0.14 & 0 & 0.19 & 0.64 & 0.05 \\ 0.25 & 0.25 & 0.19 & 0 & 0.75 & 0.16 \\ 0.7 & 0.7 & 0.64 & 0.75 & 0 & 0.61 \\ 0.11 & 0.11 & 0.05 & 0.16 & 0.61 & 0 \end{bmatrix}$$

In the IU matrix $\mathbf{\Delta}(m_1)$, we see that the union of θ_1 and θ_2 has the greatest impact on the BBA $m_1(\cdot)$, so these two focal elements will be merged first in the following multi-granular mapping. For the BBA $m_2(\cdot)$, θ_4 and θ_5 will be merged because the union of these two focal elements in the IU matrix $\mathbf{\Delta}(m_2)$ has the greatest impact. Then, in the adjacency matrices $\mathbf{AM}(m_1)$ and $\mathbf{AM}(m_2)$, the positions of these selected focal elements are marked as 1, and the others are set as 0. Besides, in order to compare with the traditional construction method for adjacency matrix (7), we set different threshold (ρ) values and observe the corresponding adjacency matrices $\mathbf{AM}_{\rho=0.4}(m_1)$ and $\mathbf{AM}_{\rho=0.4}(m_2)$, respectively. Clearly, these derived adjacency matrices have obvious differences with the change of threshold (ρ). Through the graphical visualization of all adjacency matrices in Fig.2, it can be seen that by selecting the maximum value in IU instead of the threshold (ρ) setting, those focal elements requiring aggregation can be quickly detected for the subsequent multi-granular mapping.

$$\mathbf{AM}(m_1) = \begin{bmatrix} 0 & 1 & 0 & 0 & 0 & 0 \\ 1 & 0 & 0 & 0 & 0 & 0 \\ 0 & 0 & 0 & 0 & 0 & 0 \\ 0 & 0 & 0 & 0 & 0 & 0 \\ 0 & 0 & 0 & 0 & 0 & 0 \\ 0 & 0 & 0 & 0 & 0 & 0 \end{bmatrix}$$

$$\mathbf{AM}(m_2)=\begin{bmatrix} 0 & 0 & 0 & 0 & 0 & 0 \\ 0 & 0 & 0 & 0 & 0 & 0 \\ 0 & 0 & 0 & 0 & 0 & 0 \\ 0 & 0 & 0 & 0 & 1 & 0 \\ 0 & 0 & 0 & 1 & 0 & 0 \\ 0 & 0 & 0 & 0 & 0 & 0 \end{bmatrix}$$

$$\mathbf{AM}_{\rho=0.4}(m_1)=\begin{bmatrix} 0 & 1 & 1 & 1 & 1 & 1 \\ 1 & 0 & 0 & 0 & 0 & 0 \\ 1 & 0 & 0 & 0 & 0 & 0 \\ 1 & 0 & 0 & 0 & 0 & 0 \\ 1 & 0 & 0 & 0 & 0 & 0 \\ 1 & 0 & 0 & 0 & 0 & 0 \end{bmatrix}$$

$$\mathbf{AM}_{\rho=0.4}(m_2)=\begin{bmatrix} 0 & 0 & 0 & 0 & 1 & 0 \\ 0 & 0 & 0 & 0 & 1 & 0 \\ 0 & 0 & 0 & 0 & 1 & 0 \\ 0 & 0 & 0 & 0 & 1 & 0 \\ 1 & 1 & 1 & 1 & 0 & 1 \\ 0 & 0 & 0 & 0 & 1 & 0 \end{bmatrix}$$

C. Multi-Granular Mapping of Focal Elements

Once the adjacency matrix between focal elements is obtained, discovering the existing communities between focal elements can be implemented. In this paper, two specific communities are conducted: the decision-making community and the supporting community. After that, focal elements within the decision-making community can be selected to achieve multi-granular mapping. Assuming that there exist two pairs of focal elements $\{X_{i1}, X_{j1}\}$ and $\{X_{i2}, X_{j2}\}$ in a piece of evidence belonging to two different communities, the aggregated coarse-grained focal elements Y_1, Y_2 and the belief masses can be constructed as follows:

$$\begin{aligned} Y_1 &= X_{i1} \cup X_{j1} = \{X_{i1}, X_{j1}\}; \\ Y_2 &= X_{i2} \cup X_{j2} = \{X_{i2}, X_{j2}\}; \end{aligned} \tag{9}$$

and

$$\begin{cases} \hat{m}(Y_1) = m(Y_1) + m(X_{i1}) + m(X_{j1}), \\ \hat{m}(X_{i1}) = 0, \\ \hat{m}(X_{j1}) = 0. \end{cases} \tag{10}$$

$$\begin{cases} \hat{m}(Y_2) = m(Y_2) + m(X_{i2}) + m(X_{j2}), \\ \hat{m}(X_{i2}) = 0, \\ \hat{m}(X_{j2}) = 0. \end{cases} \tag{11}$$

Then, if $\hat{m}(Y_1) > \hat{m}(Y_2)$, we regard the specific community consisting of X_{i1} and X_{j1} as the decision-making community. Meanwhile, X_{i2} and X_{j2} are in the supporting community. Finally, the focal elements and their corresponding belief masses in the final multi-granular source of evidence can be determined as follows:

$$\tilde{m}(X_{i1}) = m(X_{i1}) + \frac{1}{2} * \hat{m}(Y_2). \tag{12}$$

$$\tilde{m}(X_{j1}) = m(X_{j1}) + \frac{1}{2} * \hat{m}(Y_2). \tag{13}$$

Regarding the detection of the communities within focal elements, we only consider two groups of communities here: the connected communities between focal elements (the decision-making community) and the absence of connected communities between focal elements (the supporting community). According to the generation rule (8) for the adjacency matrix, communities can be easily discovered within the focal elements and then the steps of multi-granular mapping are conducted according to (9) and (10)-(13).

Example 2 (continued): since the adjacency matrices $\mathbf{AM}(m_1), \mathbf{AM}(m_2)$ corresponding to $m_1(\cdot)$ and $m_2(\cdot)$ are obtained, the graph structures of focal elements can also be derived. For $m_1(\cdot)$, there is a connection between θ_1 and θ_2 which play the most important role in making the final decision; for $m_2(\cdot)$, there exists a connection between θ_4 and θ_5, and there is no connection between the other focal elements for both $m_1(\cdot)$ and $m_2(\cdot)$. The generated two communities for $m_1(\cdot)$ and $m_2(\cdot)$ are:

$$m_1(\cdot) : X_1^1 = \{\theta_1, \theta_2\}; X_2^1 = \{\theta_3, \theta_4, \theta_5, \theta_6\}. \tag{14}$$

$$m_2(\cdot) : X_1^2 = \{\theta_4, \theta_5\}; X_2^2 = \{\theta_1, \theta_2, \theta_3, \theta_6\}. \tag{15}$$

Then, the fine-grained focal elements in the decision-making community and their corresponding belief masses generated by these two communities can be calculated as follows:

$$m_1(\cdot): \begin{array}{l} X_1^1 = \theta_1 \cup \theta_2 = \{\theta_1, \theta_2\}; \\ X_2^1 = \theta_3 \cup \theta_4 \cup \theta_5 \cup \theta_6 = \{\theta_3, \theta_4, \theta_5, \theta_6\}. \end{array} \tag{16}$$

$$m_2(\cdot): \begin{array}{l} X_1^2 = \theta_4 \cup \theta_5 = \{\theta_4, \theta_5\}; \\ X_2^2 = \theta_1 \cup \theta_2 \cup \theta_3 \cup \theta_6 = \{\theta_1, \theta_2, \theta_3, \theta_6\}. \end{array} \tag{17}$$

$$\begin{aligned} &\hat{m}_1(X_1^1) = m_1(\theta_1) + m_1(\theta_2) = 0.80; \\ &\hat{m}_1(X_2^1) = m_1(\theta_3) + m_1(\theta_4) + m_1(\theta_5) + m_1(\theta_6) = 0.20. \end{aligned} \tag{18}$$

$$\begin{aligned} &\hat{m}_2(X_1^2) = m_2(\theta_4) + m_2(\theta_5) = 0.75; \\ &\hat{m}_2(X_2^2) = m_2(\theta_1) + m_2(\theta_2) + m_2(\theta_3) + m_2(\theta_6) = 0.25. \end{aligned} \tag{19}$$

$$\begin{aligned} \tilde{m}_1(\theta_1) &= m_1(\theta_1) + \tfrac{1}{2} * \hat{m}_1(X_2^1) = 0.8; \\ \tilde{m}_1(\theta_2) &= m_1(\theta_2) + \tfrac{1}{2} * \hat{m}_1(X_2^1) = 0.2. \end{aligned} \tag{20}$$

$$\begin{aligned} \tilde{m}_2(\theta_4) &= m_2(\theta_4) + \tfrac{1}{2} * \hat{m}_2(X_2^2) = 0.275; \\ \tilde{m}_2(\theta_5) &= m_2(\theta_5) + \tfrac{1}{2} * \hat{m}_2(X_2^2) = 0.725. \end{aligned} \tag{21}$$

It can be seen in Fig.3 that the mapped multi-granular sources of evidence $\tilde{m}_1(\cdot)$ and $\tilde{m}_2(\cdot)$ contain only two sets of fine-grained focal elements, thus providing guarantee for subsequent efficient fusion.

D. Multi-Granular Fusion and Decision Making

After obtaining multi-granular sources of evidence, the PCR6 combination rule [25] can be applied to fuse the these mapped BBAs:

$$\tilde{m}_{PCR6} = PCR6\left(\tilde{m}_1, \tilde{m}_2, \cdots, \tilde{m}_N\right). \tag{22}$$

So far, in the BF community, some advanced classical techniques have been developed and widely applied in the literature to make the final decision. For example, decision based on maximum of credibility: $Bel(\cdot)$ or decision based on maximum of plausibility: $Pl(\cdot)$. Recently, a novel decision-making strategy with belief interval distance $d_{BI}(\cdot)$ was proposed in [30]. Considering the superiority of the decision technique with $d_{BI}(\cdot)$ [30, 31], we apply $d_{BI}(\cdot)$ to make the final decision after the fusion step. The calculation of the

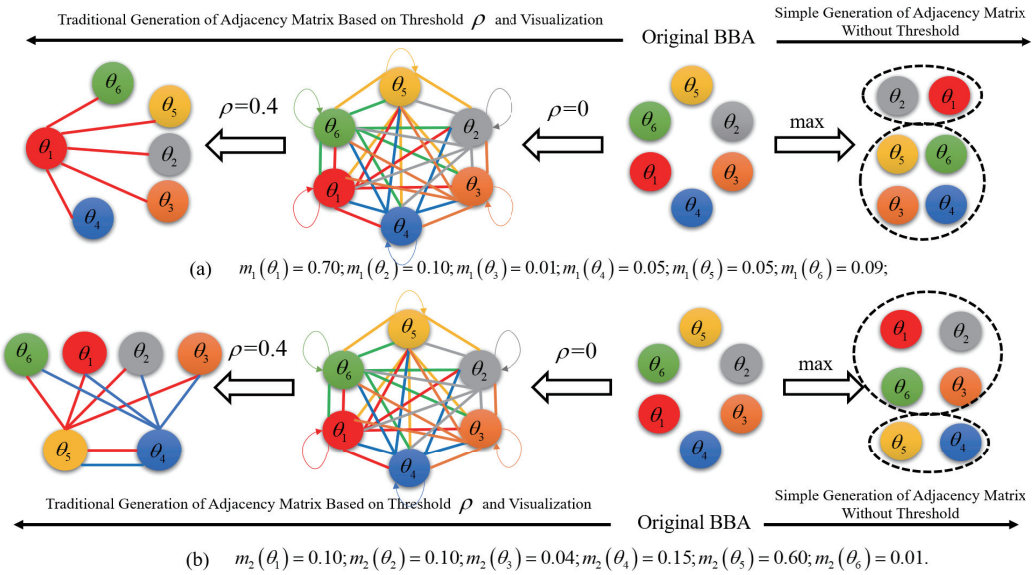

Fig. 2: Visualization of the Adjacency Matrix for $m_1(\cdot)$ and $m_2(\cdot)$.

TABLE II: Comparisons Between MGBF and Traditional PCR6-based Fusion.

	θ_1	θ_2	θ_3	θ_4	θ_5	θ_6	Final Decision
$d_{BI}(\tilde{m}_{PCR6}, m_\theta)$	**0.2725**	0.4605	0.4798	0.4482	0.3169	0.4798	θ_1
$d_{BI}(m_{PCR6}, m_\theta)$	**0.2562**	0.4608	0.4779	0.4596	0.3311	0.4715	θ_1

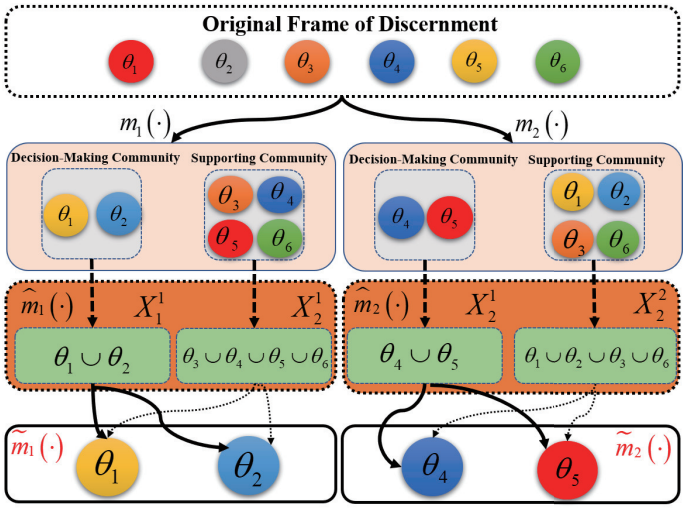

Fig. 3: **The Process of Multi-Granular Mapping for BBA Granulation.**

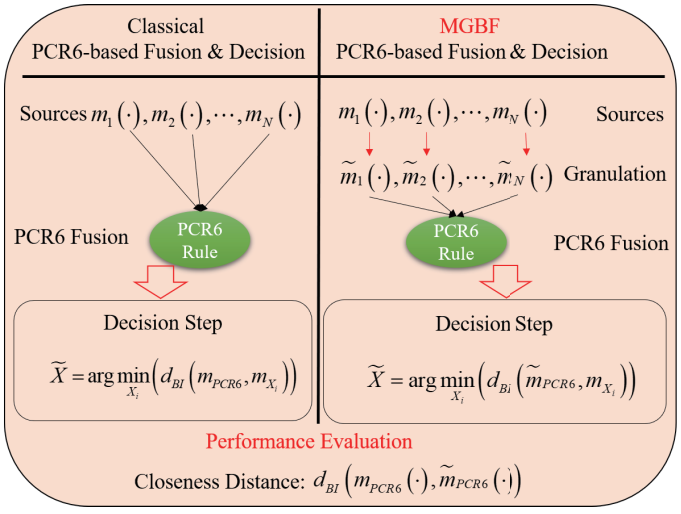

Fig. 4: **The General Principle of the Proposed MGBF Approach.**

interval distance between the BBA $m(\cdot)$ and the particular (categorial) BBA defined by $m_X(X) = 1$ of each focal element $X \in 2^\Theta$ based on $d_{BI}(\cdot)$:

$$d_{BI}(m, m_X) = \sqrt{N_c \cdot \sum_{A \in 2^\Theta} d_{BI}^2(BI(A), BI_X(A))}. \quad (23)$$

Where N_c is the normalization factor: $N_c = 1/2^{(|2^\Theta|-1)}$ to have $d_{BI}(m, m_X) \in [0, 1]$. Besides, $BI(A) : [Bel(A), Pl(A)]$, $BI_X(A) : [Bel_X(A), Pl_X(A)]$, $d_{BI}([a, b], [c, d]) = \sqrt{[\frac{a+b}{2} - \frac{c+d}{2}]^2 + \frac{1}{3}[\frac{b-a}{2} - \frac{d-c}{2}]^2}$. Besides, m_X is the particular (categorial) BBA defined by $m_X(X) = 1$ and $m_X(A) = 0$ for any $A \neq X$.

Finally, we can make the decision $\tilde{X}$ based on minimum of belief interval distance: $d_{BI}(\cdot)$:

$$\tilde{X} = \arg\min_{X \in \Theta} d_{BI}(m, m_X). \quad (24)$$

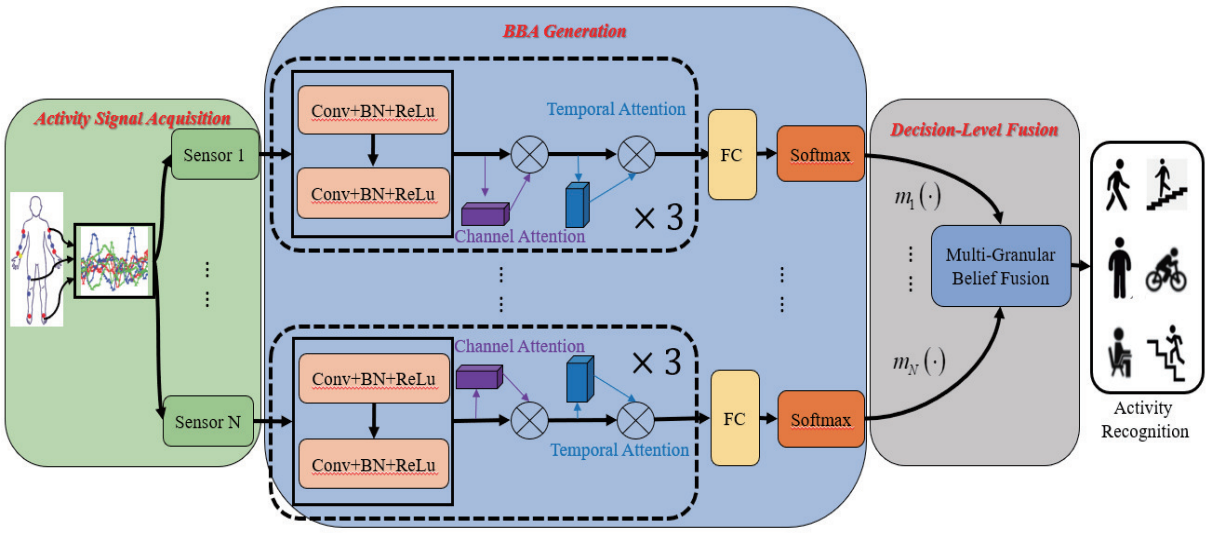

Fig. 5: Overview of the Proposed CNN+Attention Network with Multi-Granular Belief Fusion.

In order to make more clear comparisons, the general principle of the MGBF approach for fusion and decision making, and performance comparison with respect to the classical PCR6-based fusion approach are presented in Fig.4. Besides, we also use (d_{BI} (23)) to measure the closeness distance between the indirect PCR6-based fusion results after BBA granulation or approximation and the direct PCR6-based fusion results for original BBAs.

Example 2 (continued): Based on (22), the multi-granular BBA $\tilde{m}_1(\cdot)$ and $\tilde{m}_2(\cdot)$ can be easily fused and the combined BBA is given as follows:

$$\begin{array}{l} \tilde{m}_{PCR6}(\theta_1) = 0.4680; \\ \tilde{m}_{PCR6}(\theta_2) = 0.0545; \\ \tilde{m}_{PCR6}(\theta_4) = 0.0881; \\ \tilde{m}_{PCR6}(\theta_5) = 0.3894. \end{array} \tag{25}$$

Finally, we can also use (23) and (24) to obtain $d_{BI}(\tilde{m}_{PCR6}, m_\theta)$, which is given as follows:

$$d_{BI}(\tilde{m}_{PCR6}, m_{\theta_1}) = 0.2725;$$
$$d_{BI}(\tilde{m}_{PCR6}, m_{\theta_2}) = 0.4605;$$
$$d_{BI}(\tilde{m}_{PCR6}, m_{\theta_3}) = 0.4798;$$
$$d_{BI}(\tilde{m}_{PCR6}, m_{\theta_4}) = 0.4482;$$
$$d_{BI}(\tilde{m}_{PCR6}, m_{\theta_5}) = 0.3169;$$
$$d_{BI}(\tilde{m}_{PCR6}, m_{\theta_6}) = 0.4798.$$

Since $(d_{BI}(\tilde{m}_{PCR6}, m_{\theta_3}) \simeq d_{BI}(\tilde{m}_{PCR6}, m_{\theta_6})) \succ d_{BI}(\tilde{m}_{PCR6}, m_{\theta_2})) \succ (d_{BI}(\tilde{m}_{PCR6}, m_{\theta_4}) \succ d_{BI}(\tilde{m}_{PCR6}, m_{\theta_5})) \succ (d_{BI}(\tilde{m}_{PCR6}, m_{\theta_1})$, θ_1 will be the final decision. In addition, to compare the direct PCR6-based fusion with our proposed multi-granular fusion in terms of fusion accuracy and efficiency, we list the fusion results $d_{BI}(\tilde{m}_{PCR6}, m_\theta)$ and $d_{BI}(m_{PCR6}, m_\theta)$ in Table II. It can be seen from this table that the final decision result of our multi-granular fusion is consistent with the result of the classical PCR6-based fusion method, that is, the final decision is θ_1. In addition, we also give the computation time of the two fusion strategies. It can be found that the running time of the multi-granular fusion method (0.0026s) is nearly 3 times faster than that of the traditional PCR6-based fusion method (0.0071s). The corresponding d_{BI} distance between the direct PCR6 fusion result and MGBF-based fusion result is 0.0223, which indicates a very good proximity of the two results. This has been calculated by $d_{BI}(\tilde{m}_{PCR6}(\cdot), m_{PCR6}(m_1, m_2))$ (23). The interest and the effectiveness of this new MGBF approach with respect of the classical PCR6-based fusion approach is shown in the next section for the human activity recognition application.

IV. Human Activity Recognition Based on Multi-Granular Belief Fusion

Human Activity Recognition (HAR) is mainly used to maintain or improve human health by detecting and classifying human daily activities. At present, this technology has been widely used in the fields of elderly monitoring [32], sports monitoring [33], medical care [34] and so on. Generally speaking, HAR can be divided into vision-based HAR and wearable sensor-based HAR. Considering that the accuracy of vision-based HAR is easily affected by environmental noise such as illumination or overlap between subjects, wearable sensor-based HAR has attracted more and more attention from researchers [5, 35]. Therefore, in this work, we mainly focus our discussions on wearable sensor based HAR, and comprehensively discuss the effectiveness of the proposed multi-granular belief fusion method from two aspects: the accuracy of activity recognition and the fusion efficiency.

A. Overview of the MGBF based Activity Recognition Model

In this work, with the help of the end-to-end learning ability of the CNN+Attention model proposed by Gao et al. [36], we present the multi-granular belief fusion (MGBF)

model to complete high-precision activity recognition. The framework of the MGBF-based activity recognition model with the basic CNN+Attention model is shown in Fig.5, which mainly includes the following three steps:

- Step 1: divide the original dataset into several separate parts based on the type of sensors in body sensor networks. In the following discussions, the original dataset is only divided into two simple parts: accelerometer-based sensor perception data and gyroscope-based sensor perception data;
- Step 2: with the help of the end-to-end CNN+Attention basic model, BBA acquisition of activity categories is realized. It is worth noting that the number of the derived BBAs is determined by the number of CNN+Attention basic models, which are trained by the divided datasets;
- Step 3: the outputs of the CNN+Attention models are combined by the proposed multi-granular belief fusion method, and finally, the unknown class of the activity can be predicted.

B. End-to-End CNN+Attention Network for the Output of BBA

Compared with our earlier works based on manual features engineering [4], the deep end-to-end architecture has the capacity of automatic feature extraction, thus ensuring the effectiveness of feature engineering and the high-precision of action recognition. At present, more and more activity recognition models rely on the deep learning framework [37]. In this paper, we follow this deep learning-based line, and the base model in the proposed multi-granular belief fusion model is the CNN+Attention network, which was initially proposed in [36]. The structure of the CNN+Attention network is shown in Fig.5, which mainly includes a convolutional layer, a channel attention sub-module, and a temporal attention sub-module. The training process of the CNN+Attention model is mainly divided into three steps: firstly, with the help of a fixed-length sliding window, the time series data is divided into a set of short signals along the time axis. Then, the acquired signals are fed into a convolutional layer to extract the deep features; Secondly, in the channel attention module, the derived features are aggregated using the max pooling and average pooling methods. Then, the sigmoid function is used to generate probabilities; Thirdly, in the temporal attention, the channel information across channel axes is aggregated by applying max pooling and average pooling techniques to generate subsequent temporal attention maps; Finally, the feature vector is fed into the fully connected (FC) layer and then the outputs of the softmax layer will be regarded as the corresponding BBAs.

1) Channel Attention Module: Suppose a convolution layer and its generated feature map: $F \in R^{Cl\times H\times W}$, where Cl, W and H represent the dimensions of channel (i.e. number of filters), width (temporal axis) and height (sensor axis), respectively. In order to effectively calculate channel attention, for a given input feature, the weight of channel attention can be calculated as:

$$W_{Cl} = \sigma\left(w_2 \mathrm{Re}LU\left(w_1 g_1\left(F\right)\right) + w_2 \mathrm{Re}LU\left(w_1 g_2\left(F\right)\right)\right). \tag{26}$$

where $g_1 = \frac{1}{WH}\sum_{i=1,j=1}^{W,H} F_{ij}, g_2 = \max_{i=1,j=1}^{W,H} F_{ij}$ represent the global average pooling and max pooling of the channel, respectively; $\sigma\left(\cdot\right)$ is the sigmoid function; $\mathrm{Re}LU\left(\cdot\right)$ is the rectified linear unit [38]; $w_1 = Cl\times(Cl/r)\,; w_2 = (Cl/r)\times Cl$ and r is the reduction rate of the convolutional layer.

2) Temporal Attention Module: Similar to the computation of the channel attention submodule, the computation of temporal attention can concatenate the channel information of features through max-pooling and average-pooling operations. Here, we concatenate the information by connecting two pooled features, and normalize the convolution of the channel information. The specific calculation method is as follows:

$$W_T = \sigma\left(f^{scf\times 1}\left(\left[g_1\left(F\right); g_2\left(F\right)\right]\right)\right). \tag{27}$$

where $\sigma\left(\cdot\right)$ is the sigmoid function; $scf \times 1$ represents the size of the convolution filter; g_1, g_2 is the average pooling and max pooling; here, the size of filter is set to: $scf \times 1 = 7 \times 1$.

More details about the CNN+Attention network can be found in [36]. Here, we mainly use this classical network as the base model for our proposed multi-granular belief fusion framework to verify the effectiveness of this new approach.

C. Experiments

1) Data Set Description: In the HAR field, the two public datasets: UCI Smartphone dataset[4] and OPPORTUNITY[5] are widely used. The UCI Smartphone dataset mainly includes six activities (sitting, standing, laying, walking, walking upstairs and downstairs), which were repeated by thirty subjects throughout the data collection process. More details about Smartphone can be found in [39]. For the OPPORTUNITY dataset [40], it records the real-world daily living activities of 12 subjects in a sensor-rich environment. The sensory data were collected from IMUs attached to 12 body locations, namely upper limbs, back and feet. The resulting dataset has 79 dimensions and in this paper, we aim to use our proposed model to classify the involved 18 daily activities in this dataset.

2) Experimental Setup: As discussed earlier, the multi-granular belief fusion recognition model proposed here cannot be directly applied to raw time series of daily activities. Therefore, a sliding window technique is first applied to the raw time series data. The sliding window length here is set to 8 and the sliding step is set to 2. The dataset was randomly split into a 70% training set and a 30% testing set. The Adam optimization is used to train the network with a batch size of 150. The initial learning rate is set to 0.001 and will decrease by a factor of 0.1 after every 30 epochs; For the OPPORTUNITY dataset, since it has a significantly unbalanced class distribution and an additional strong bias towards NULL classes, the NULL classes are considered when evaluating the performance of our proposed MGBF-based recognition model. Here, we replicate the same training and testing steps from [36]. The runs 2, 4, and 5 from subject 1, 2, and 3 are used as the test set, the other data are used as training set. Moreover, the sliding

[4]Online. [Available]: http://archive.ics.uci.edu/ml/datasets/Smartphone-Based+Recognition+of+Human+Activities+and+Postural+Transitions.

[5][Online]. Available: http://archive.ics.uci.edu/ml/datasets/ OPPORTUNITY+Activity+Recognition.

TABLE III: Brief Description for CNN+Attention Network.

Layer	Layer 1	Layer 2	Layer 3		
CNN+Attention	Conv,128 Conv,128 AttModule	Conv,256 Conv,256 AttModule	Conv,384 Conv,384 AttModule	FC	Softmax

window length is set to 84 and the sliding step is set to 8. And in the training process, the batch size is set to 150. We set the initial learning rate to 0.001, which will decrease by a factor of 0.1 after every 30 epochs. The specific structure of CNN+Attention Network is shown in Table III.

3) Measure of Performances: In this paper, we use $Accuracy$ to measure the performance of the proposed MGBF-based model, which is defined by [41]

$$Accuracy = \frac{1}{n}\sum_{h=1}^{n}\frac{TP_h + TN_h}{TP_h + TN_h + FP_h + FN_h}. \quad (28)$$

where h denotes class index and n is the number of classes. TP_h, TN_h, FP_h and FN_h are respectively True Positives: TP, True Negatives: TN, False Positives: FP and False Negatives: FN.

4) Results on the UCI Smartphone Dataset: In Fig.6, the train and test error curves of the MGBF-based model on Smartphone are first presented. It can be clearly seen that with the increase in the number of iterations, the training error and test error of our proposed model gradually tend to the minimum value. We also give the confusion matrix of activity recognition in Fig.7. It can be observed that even for similar activities such as walking upstairs and downstairs, the proposed MGBF-based model can also effectively identify these activities. The performance of this high-precision activity recognition mainly depends on two aspects: 1. deep feature extraction based on the CNN+Attention network; 2. multi-granular belief fusion. Furthermore, we compare the recognition results of the MGBF-based model with other classical methods. A comprehensive list of recognition models for the UCI Smartphone dataset published in the literature is shown in Table IV, including Hyperbox Neural Networks [42], FW K-Nearest Neighbor [43], FW Naive Bayes [43], Neural Networks with Incremental Supervised Learning [44], Stacked Denoising Autoencoders [45], DSmT-KDE [46], etc. The results show that our method achieves an average 3% improvement in accuracy compared to traditional activity recognition models based on classical approaches. Moreover, we are also able to observe that the performance of the MGBF-based recognition model is the best among all the mentioned algorithmic models.

To further discuss and verify the effectiveness of our fusion algorithm, we comprehensively compare the performance of the multi-granular belief fusion based on graph structure and the classical PCR6 rules from three aspects: recognition accuracy, degradation (i.e. closeness distance), and computation time of fusion. As can be seen from Fig.8, compared with the PCR6 fusion rule, the degradation of the multi-granular fusion algorithm remains within an acceptable range (0.0278 ± 0.0178). The most interesting and attractive phenomenon is that such degradation does not cause the loss of activity recognition accuracy (96.05%) with respect to the classical PCR6 fusion (96.05%), but its fusion efficiency in terms of computation time saving is increased by more than five times from the perspective of computation time (multi-granular fusion: 0.1296 ± 0.0503 ms; traditional PCR6: 0.6301 ± 0.2529 ms). This result further shows that such information loss has no impact on the decision results and also proves that our proposed multi-granular belief fusion algorithm is feasible and effective.

TABLE IV: Comparison of the Proposed Method with the State-of-The-Art Approaches on the UCI Smartphone dataset.

Method	Accuracy
Hyperbox Neural Network [42]	87.4%
FW K-Nearest Neighbor [43]	87.8%
FW Naive Bayes [43]	90.1%
Neural Network with Incremental Supervised Learning [44]	92.83%
Stacked Denoising Autoencoders [45]	91.95%
DSmT-Based Kernel Density Estimation [46]	93.05%
Our Proposed Method (PCR6)	**96.05%**
Our Proposed Method (Multi-Granular Belief Fusion)	**96.05%**

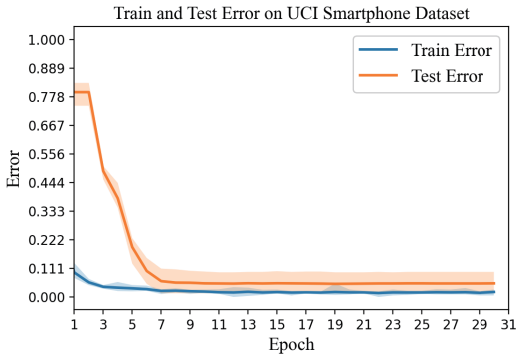

Fig. 6: **Train and test error on UCI Smartphone dataset.**

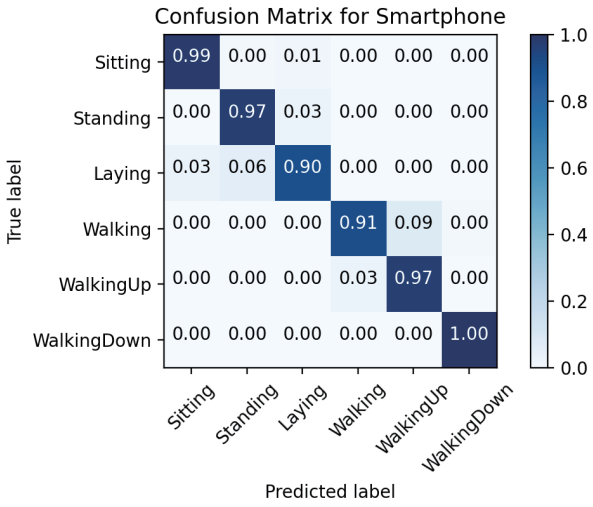

Fig. 7: **Confusion Matrix for UCI Smartphone Dataset.**

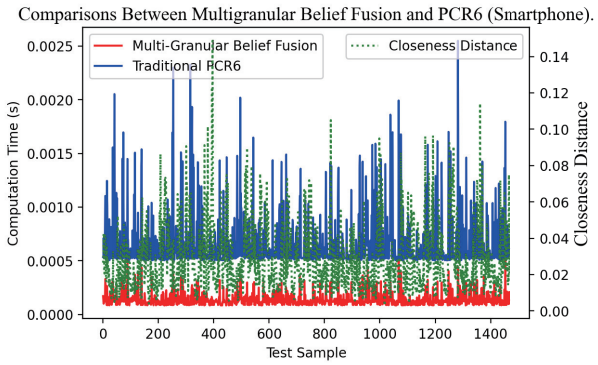

Fig. 8: **Comparisons Between Multi-granular Belief Fusion and PCR6 from Two Aspects: Computation Time and Closeness Distance (Smartphone).**

5) Results on the UCI OPPORTUNITY Dataset: Similar to the experimental results obtained with Smartphone dataset, we also give the confusion matrix of activity recognition in Fig.9. Compared with UCI Smartphone dataset, there is a total of 18 categories of activities that need to be recognized, which is much more difficult than the recognition of smartphone activities. As we can see from Fig.10(a), the opportunity dataset is an imbalanced dataset, in which A1 (NULL) accounts for 83% and the other 17 categories account for about 17%. The recognition accuracy of each activity is drawn in Fig.10(b), and we can see that the recognition accuracy of A1 (NULL) is the highest, reaching 98.1871%, while the recognition accuracy of A11 (Close Drawer1) is the worst: 12.5%. Furthermore, we compare the recognition results of the MGBF-based model with other classical methods. A comprehensive list of recognition models for the UCI Opportunity dataset published in the literature is shown in Table V, including the literature Standard Recurrent Network [47], CNN [48], CNN+LSTM [49], Layer-wise Deep Neural Networks [50], Att-based Residual Network [36], DSmT-KDE [46]etc. The results show that the performance of the multi-granular fusion recognition model is the best among all the mentioned algorithmic models.

To further discuss and verify the effectiveness of our fusion algorithm, we comprehensively compare the performance of the multi-granular belief fusion based on graph structure and the classical PCR6 rule from three aspects: recognition accuracy, closeness distance, and computation time of fusion. As can be seen from Fig.11, compared with the PCR6 fusion rule, the degradation of the results produced by the MGBF with respect to classical direct PCR6-based fusion also remains within an acceptable range (0.0119 ± 0.0125). The loss of activity recognition accuracy caused by this closeness distance is about 0.03%, but its computation time is more than 50 times from the perspective of computation time (multi-granular fusion: 0.1564 ± 0.0565 ms; traditional PCR6: 7.9204 ± 3.3116 ms). This result further proves that our proposed MGBF is feasible and effective.

6) Comparisons Between PCR6-Based MGBF and BBA Approximations: Here, we discuss the similarities and differences between the PCR6-based MGBF and three classical BBA approximations (k-l-x method [15], Summarization [16] and Non-redundancy method [51]). The relationship between PCR6-based MGBF and BBA approximation can be clearly observed from three aspects: closeness distance, computation time and accuracy of activity recognition. Among them, the computation time refers to the time required for PCR6-based fusion after granulation or approximation. As we can observe from Fig.12 with the UCI Smarphone or Opportunity dataset, the proposed MGBF and classical BBA approximation methods exhibit some similar and some different characteristics, which can be summarized as the following points:

- Similarities:
  - Both the proposed MGBF and classical BBA approx-

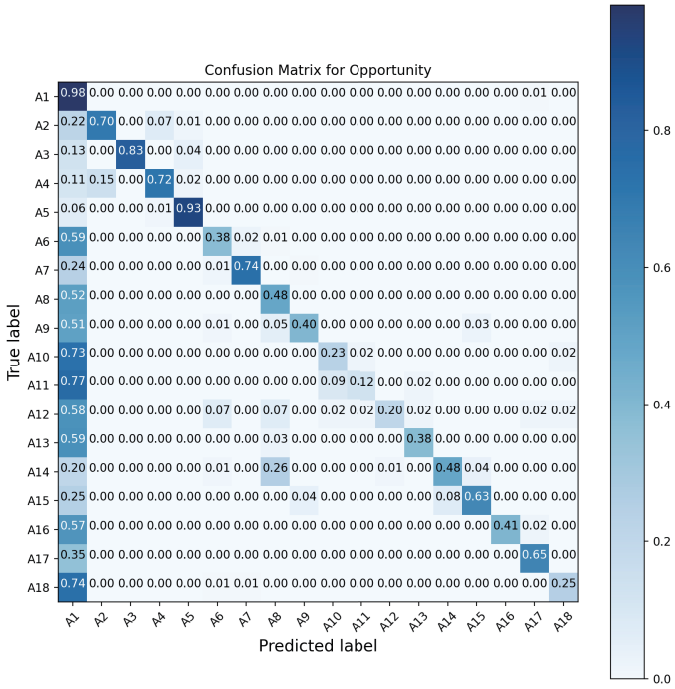

Fig. 9: **Confusion Matrix for UCI Opportunity Dataset. (A1: NULL; A2: Open Door1; A3: Open Door2; A4: Close Door1; A5: Close Door2; A6: Open Fridge; A7: Close Fridge; A8: Open Dishwater; A9: Close Dishwater; A10: Open Drawer1; A11: Close Drawer1; A12: Open Drawer2; A13: Close Drawer2; A14: Open Drawer3; A15: Close Drawer3; A16: Clearn Table; A17: Drink from Cup; A18: Toggle Switch.)**

TABLE V: Comparison of the Proposed Methd with the State-of-The-Art Approaches on the UCI Opportunity dataset.

Method	Accuracy
Standard Recurrent Network [47]	74.5%
Standard CNN [48]	76.83%
CNN+LSTM [49]	78.90%
Layer-wise Deep Neural Networks [50]	81%
Att-based Residual Network [36]	82.75%
Our Proposed Method (PCR6)	**90.85%**
Our Proposed Method (Multi-Granular Belief Fusion)	**90.82%**

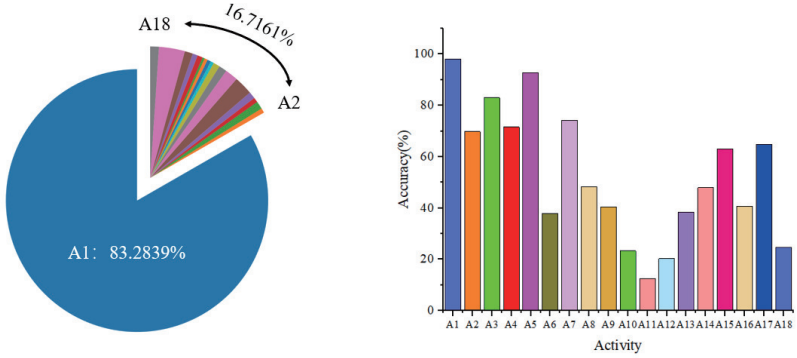

(a) Proportion of Each Category in the Test Set. (b) Accuracy for Each Category in the Test Set.

Fig. 10: **Proportion and the Corresponding Accuracy of Each Category in the Test Set (Opportunity).**

TABLE VI: Comparison of Classical Fusion Approaches with Our Proposed MGBF Strategy on the UCI Smartphone dataset.

	Original Direct Fusion		The Proposed MGBF-Based Fusion		
-	Accuracy (%)	Computation Time (ms)	Accuracy (%)	Computation Time (ms)	Information Loss
Yager's Rule	94.15	0.3838 ± 0.1318	93.61 ($\downarrow$ 0.54%)	0.0877 ± 0.0266 ($\uparrow$ 77.15%)	0.1130 ± 0.0559
Murphy's Rule	88.49	0.3903 ± 0.1502	88.35 ($\downarrow$ 0.14%)	0.0920 ± 0.0375 ($\uparrow$ 76.43%)	0.1160 ± 0.0543
Dempster's Rule	95.92	0.6487 ± 0.2327	95.71 ($\downarrow$ 0.21%)	0.1099 ± 0.0424 ($\uparrow$ 83.06%)	0.0281 ± 0.0449
PCR6	96.05	0.6301 ± 0.2529	96.05 ($\downarrow$ 0%)	0.1296 ± 0.0503 ($\uparrow$ 79.43%)	0.0278 ± 0.0178

TABLE VII: Comparison of Classical Fusion Approaches with Our Proposed MGBF Strategy on the UCI Opportunity dataset.

	Original Direct Fusion		The Proposed MGBF-Based Fusion		
-	Accuracy (%)	Computation Time (ms)	Accuracy (%)	Computation Time (ms)	Information Loss
Yager's Rule	88.58	5.4716 ± 2.7553	88.49 ($\downarrow$ 0.09%)	0.1102 ± 0.0376 ($\uparrow$ 97.99%)	0.0646 ± 0.0433
Murphy's Rule	90.82	5.5304 ± 3.8232	88.49 ($\downarrow$ 2.33%)	0.1118 ± 0.0402 ($\uparrow$ 97.98%)	0.0613 ± 0.0397
Dempster's Rule	90.74	6.5871 ± 3.5769	88.99 ($\downarrow$ 1.85%)	0.1344 ± 0.0472 ($\uparrow$ 97.96%)	0.0159 ± 0.0441
PCR6	90.85	7.9204 ± 3.3116	90.82 ($\downarrow$ 0.03%)	0.1564 ± 0.0565 ($\uparrow$ 98.03%)	0.0119 ± 0.0125

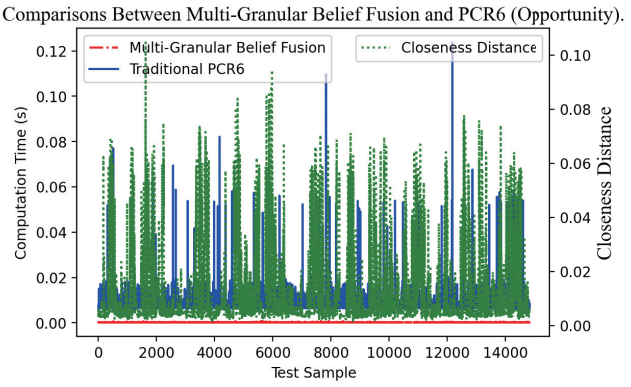

Fig. 11: **Comparisons Between Multi-Granular Belief Fusion and PCR6 from Two Aspects: Computation Time and Closeness Distance (Opportunity).**

imations bring a certain degree of closeness distance, which can be seen in Fig.12.(1) and Fig.12.(4). Among them, the degradation of BBA approximation increases with the decrease of the number of remaining focal elements;

– Both the proposed MGBF and classical BBA approximations can reduce the computational complexity of fusion, that is, the computation time required for fusion rules is significantly reduced, which can be observed in Fig.12.(2) and Fig.12.(5). Among them, the computation time of the BBA approximation methods decreases gradually with the reduction of the number of remaining focal elements;

– Both the proposed MGBF and BBA approximation will lead to the reduction of classification accuracy; Among them, with the decrease of the remaining focal elements, the classification accuracy of BBA approximations will also gradually decrease.

- Differences:
  – From an approximation point of view, it is wise and prudent to change the original BBA gradually and slightly, which aims to guarantee sufficient overall similarity compared to the original BBA. However, the MGBF method proposed here emphasizes the preservation of the decision information in the original BBA, and at the same time, the unimportant focal elements are aggregated at one time, thus avoiding the step-by-step discussion of the deletion of focal elements. As we can see in Fig.12.(3) and Fig.12.(6), MGBF can effectively ensure the recognition accuracy while improving the fusion efficiency;
  – In practical applications, especially for problems with large FoD, the step-by-step sequential deletion of focal elements in classical BBA approximation is too cautious. As can be seen in Fig.12.(6), when the number of the remaining focal elements is reduced from 18 to 6,

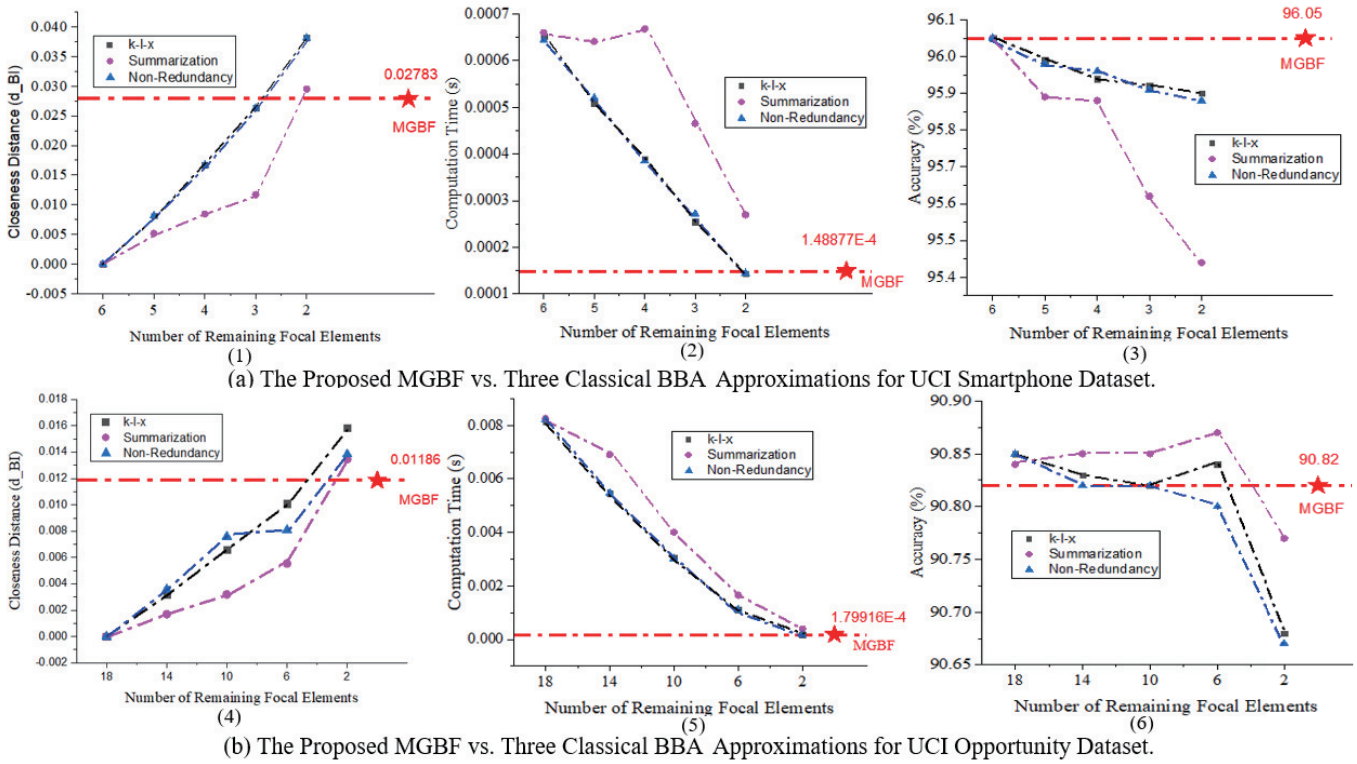

Fig. 12: **PCR6-based MGBF and classical BBA Approximation Methods for UCI Smartphone and Opportunity Datasets.**

the classification accuracy of activities does not change significantly. However, the corresponding closeness distance in Fig.12.(6) has been increasing. That is to say, the lost information comes from those unimportant focal elements that have no decisive influence on the final decision. The motivation of BBA granulation is to avoid the step-by-step discussion about the deletion of unimportant (non-decision-making) focal elements, and to retain those focal elements with decision attributes as much as possible, which is very meaningful for practical problems under the large FoD.

7) Comparisons Between Different Fusion Rules in MGBF: As we have already described in Section III.D and Fig.4, the proposed MGBF strategy in this paper is to reduce the computational complexity of classical fusion rules in the belief functions community with the help of the novel multi-granular mapping approach. To further prove the effectiveness of the MGBF, more comprehensive comparisons have been given here to observe whether the multi-granular mapping is effective by changing the basic classical fusion rules in MGBF. Four classical fusion rules are considered: Yager's Rule [52], Murply's Rule [53], Dempster's Rule (3) and the PCR6 (4). The comparison results are given in Table VI and Table VII. As we can see in these two tables, in general, with the help of the multi-granular mapping strategy, the computational efficiency of all classical fusion rules has been significantly improved. The cost of such efficiency improvement is the decline of activity recognition accuracy caused by information loss within the acceptable range. The original intention of the multi-granular fusion method is to avoid the impact of activity recognition accuracy as much as possible and improve the fusion efficiency. Therefore, the smaller value after the downward arrow in the accuracy column of Table VI and Table VII is, the better (less influence on accuracy). Similarly, the larger value after the upward arrow in the computation time column is, the better (greater fusion efficiency improvement). Specifically, PCR6 rule-based MGBF has the highest accuracy in both UCI smartphone (96.05%) and opportunity (90.82%) datasets compared to other mentioned rules based multi-granular fusion methods. Compared with the original PCR6 rule, the fusion efficiency on the two data sets has increased by 79.43% and 98.03%, respectively. In addition, as discussed before, multi-granular mapping will bring about information loss to a certain extent. It can be found that both fusion rules on Smartphone and Opportunity datasets have a certain degree of decline after using multi-granular mapping. Among all mentioned classical fusion rules, the PCR6-based MBGF brings the lowest information loss in both two datasets. Although four different fusion rules have been adopted and discussed in our MGBF for activity recognition problems, the proposed multi-granular mapping strategy can still reduce the computational complexity, which proves the effectiveness and generality of our proposed method in this paper.

8) Further Discussions: In Fig.8 and Fig.11, there exist several abnormal points in the closeness distance curve, where the values of distance are relatively large and far exceed the average value. In order to explain this problem, more deep investigations are given in this part. Specifically, two representative BBAs in Fig.8 are selected: $\mathbf{m}_1(\cdot)$ with the largest

closeness distance (0.1486) is $m_1(\theta_1) = 0.0581; m_1(\theta_2) = 0.0777; m_1(\theta_3) = 0.0635; m_1(\theta_4) = 0.1993; m_1(\theta_5) = 0.2919; m_1(\theta_6) = 0.3095$ and $\mathbf{m}_2(\cdot)$ with the relative smaller distance value (0.0096) is $m_2(\theta_1) = 0.0117; m_2(\theta_2) = 0.0099; m_2(\theta_3) = 0.0116; m_2(\theta_4) = 0.0124; m_2(\theta_5) = 0.0065; m_2(\theta_6) = 0.9479$. Compared to $\mathbf{m}_1(\cdot)$, $\mathbf{m}_2(\cdot)$ is more specific with less uncertainty, which means that most belief masses are assigned to single focal element: θ_6. Thus, we give the assumption that the higher the degree of uncertainty in BBAs, the greater the closeness distance brought by the multi-granular mapping strategy. In order to verify this assumption, we adopt a classical uncertainty measure for BBAs: Probabilistic Information Content (PIC) [54]. If $m(\cdot)$ is a Bayesian BBA, for $\Theta = \{\theta_1, \theta_2, \cdots, \theta_N\}$, its PIC value is defined as[6]:

$$PIC(m) \triangleq 1 + \frac{1}{log_2 N} \sum_{i=1}^{N} m(\theta_i) log_2 m(\theta_i). \qquad (29)$$

The value of PIC metric belongs to the interval [0,1]. When the BBA is $m(\theta_i) = \frac{1}{N}$ for $i = 1, 2, \cdots, N$ in FoD Θ, the value of PIC is minimum, i.e. $PIC(m) = PIC_{min} = 0$. This case means that decision maker cannot make the final decision because all the belief masses of focal elements are the same and the degree of uncertainty is the largest. On the contrary, when the BBA is deterministic, that is, if there exists an element θ_i in Θ such as $m(\theta_i) = 1$, the PIC metric is maximum, i.e. $PIC(m) = PIC_{max} = 1$. We thus draw the relationship between PIC value and the closeness distance for UCI Smartphone and Opportunity datasets in Fig.13 and Fig.14. As we can see in these two figures, when the PIC value of the BBA is small, the closeness distance between traditional PCR6 and MGBF is larger than other BBAs with higher PIC value. Therefore, we can conclude that MGBF strategy proposed here is a multi-granular mapping method, which can reduce the uncertainty of the original BBA, thus making the final decision more specific.

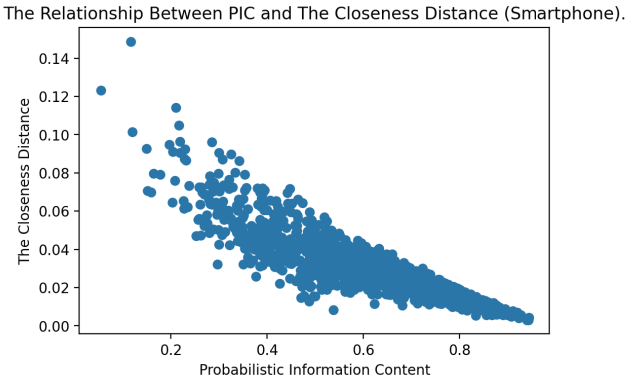

Fig. 13: **The Relationship Between PIC value and The Closeness Distance (Smartphone).**

V. Conclusion and Future Works

In this paper, we have proposed a novel efficient graph-based multi-granular belief fusion approach for human activity recognition. Compared to existing works, the CNN+Attention network is regarded as the base classifier for providing the corresponding BBAs. Then, these BBAs are fused with the multi-granular belief fusion and the final decisions can be made precisely. Based on extensive experiments on two publicly available activity classification datasets, our results show that the proposed multi-granular fusion method is more efficient than the traditional PCR6 rule. Also, the fused recognition model is superior to other advanced models for activity recognition. In future work, we will focus on researching more robust multi-criteria methods for evaluating the relationship between focal elements in BBA granulation. We will also try more intelligent local community detection algorithms in the complex network to find influential nodes in the evidence and the appropriate dimension of granularity in BBA granulation and test improved rules of combination.

[6]where $0log_2(0) = 0$ by definition.

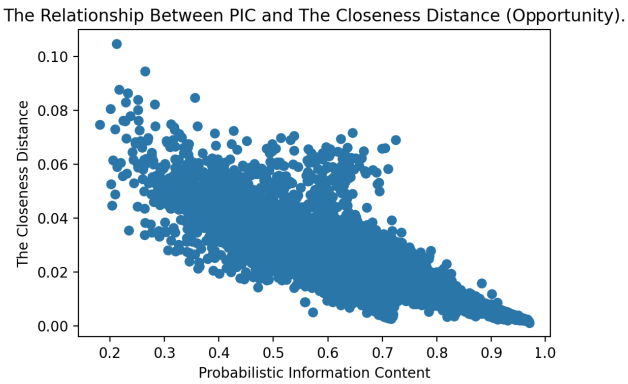

Fig. 14: **The Relationship Between PIC value and The Closeness Distance (Opportunity).**

Acknowledgment

The authors thank the reviewers and editors for giving valuable comments, which are very helpful for improving this manuscript.

References

[1] Y. Xu, Y. Li, Y. Wang, D. Zhong, and G. Zhang, "Improved few-shot learning method for transformer fault diagnosis based on approximation space and belief functions," *Expert Systems with Applications*, vol. 167, pp. 114–135, 2021.

[2] C. Zhu and F. Xiao, "A belief hellinger distance for D–S evidence theory and its application in pattern recognition," *Engineering Applications of Artificial Intelligence*, vol. 106, pp. 1044–1187, 2021.

[3] L.-H. Yang, J. Liu, Y.-M. Wang, C. Nugent, and L. Martínez, "Online updating extended belief rule-based system for sensor-based activity recognition," *Expert Systems with Applications*, vol. 186, pp. 135–173, 2021.

[4] Y. Dong, X. Li, J. Dezert, R. Zhou, C. Zhu, L. Wei, and S. S. Ge, "Evidential reasoning with hesitant fuzzy belief structures for human activity recognition," *IEEE Transactions on Fuzzy Systems*, vol. 29, no. 12, pp. 3607–3619, 2021.

[5] S. Qiu, H. Zhao, N. Jiang, Z. Wang, L. Liu, Y. An, H. Zhao, X. Miao, R. Liu, and G. Fortino, "Multi-sensor information fusion based on machine learning for real applications in human activity recognition: State-of-the-art and research challenges," *Information Fusion*, vol. 80, pp. 241–265, 2022.

[6] Y. Dong, X. Li, J. Dezert, R. Zhou, C. Zhu, and S. S. Ge, "Multi-criteria analysis of sensor reliability for wearable human activity recognition," *IEEE Sensors Journal*, vol. 21, no. 17, pp. 19 144–19 156, 2021.

[7] P. Roy, C. Chowdhury, M. Kundu, D. Ghosh, and S. Bandyopadhyay, "Novel weighted ensemble classifier for smartphone based indoor localization," *Expert Systems with Applications*, vol. 164, pp. 37–58, 2021.

[8] D. Alshamaa, F. M. Chehade, and P. Honeine, "A hierarchical classification method using belief functions," *Signal Processing*, vol. 148, pp. 68–77, 2018.

[9] Z.-G. Liu, L.-Q. Huang, K. Zhou, and T. Denœux, "Combination of transferable classification with multisource domain adaptation based on evidential reasoning," *IEEE Transactions on Neural Networks and Learning Systems*, vol. 32, no. 5, pp. 2015–2029, 2021.

[10] F. Xiao, "CED: A distance for complex mass functions," *IEEE Transactions on Neural Networks and Learning Systems*, vol. 32, no. 4, pp. 1525–1535, 2021.

[11] Y. Yi, D. Han, and J. Dezert, "Basic belief assignment approximations using degree of non-redundancy for focal element," *Chinese Journal of Aeronautics*, vol. 32, no. 11, pp. 2503–2515, 2019.

[12] R. Jiroušek, "Local computations in Dempster–Shafer theory of evidence," *International Journal of Approximate Reasoning*, vol. 53, no. 8, pp. 1155–1167, 2012.

[13] J. Klein, S. Destercke, and O. Colot, "Interpreting evidential distances by connecting them to partial orders: Application to belief function approximation," *International Journal of Approximate Reasoning*, vol. 71, pp. 15–33, 2016.

[14] A. Tan, W.-Z. Wu, and Y. Tao, "A unified framework for characterizing rough sets with evidence theory in various approximation spaces," *Information Sciences*, vol. 454, pp. 144–160, 2018.

[15] B. Tessem *et al.*, "Approximations for efficient computation in the theory of evidence," *Artificial Intelligence*, vol. 61, no. 2, pp. 315–329, 1993.

[16] J. D. Lowrance, T. D. Garvey, and T. M. Strat, "A framework for evidential-reasoning systems," in *Classic Works of the Dempster-Shafer Theory of Belief Functions*. Springer, 2008, pp. 419–434.

[17] M. Bauer, "Approximations for decision making in the Dempster-Shafer theory of evidence," *arXiv preprint arXiv:1302.3557*, 2013.

[18] M. Grabisch, "Upper approximation of non-additive measures by k-additive measures—the case of belief functions." in *ISIPTA*, 1999, pp. 158–164.

[19] T. Denœux, "Inner and outer approximation of belief structures using a hierarchical clustering approach," *International Journal of Uncertainty, Fuzziness and Knowledge-Based Systems*, vol. 9, no. 04, pp. 437–460, 2001.

[20] L. Chen, Y. Deng, and K. H. Cheong, "Probability transformation of mass function: A weighted network method based on the ordered visibility graph," *Engineering Applications of Artificial Intelligence*, vol. 105, pp. 44–68, 2021.

[21] J. Dezert and A. Tchamova, "On effectiveness of measures of uncertainty of basic belief assignments," *Information & Security Journal: An International Journal*, vol. 52, 2022.

[22] J. Zhao and Y. Deng, "Complex network modeling of evidence theory," *IEEE Transactions on Fuzzy Systems*, vol. 29, no. 11, pp. 3470–3480, 2020.

[23] L. Xiong, X. Su, and H. Qian, "Conflicting evidence combination from the perspective of networks," *Information Sciences*, vol. 580, pp. 408–418, 2021.

[24] X. Su, S. Xue, F. Liu, J. Wu, J. Yang, C. Zhou, W. Hu, C. Paris, S. Nepal, D. Jin, Q. Z. Sheng, and P. S. Yu, "A comprehensive survey on community detection with deep learning," *IEEE Transactions on Neural Networks and Learning Systems*, pp. 1–21, 2022.

[25] F. Smarandache and J. Dezert, *Advances and applications of DSmT for information fusion*. American Research Press, 2004-2015.

[26] G. Shafer, *A mathematical theory of evidence*. Princeton university press, 1976.

[27] F. Xiao, Z. Cao, and A. Jolfaei, "A novel conflict measurement in decision-making and its application in fault diagnosis," *IEEE Transactions on Fuzzy Systems*, vol. 29, no. 1, pp. 186–197, 2020.

[28] L. Wu, P. Cui, J. Pei, and L. Zhao, *Graph Neural Networks: Foundations, Frontiers, and Applications*. Singapore: Springer Singapore, 2022.

[29] Z. Wu, S. Pan, F. Chen, G. Long, C. Zhang, and P. S. Yu, "A comprehensive survey on graph neural networks," *IEEE Transactions on Neural Networks and Learning Systems*, vol. 32, no. 1, pp. 4–24, 2021.

[30] J. Dezert, D. Han, J.-M. Tacnet, S. Carladous, and Y. Yang, "Decision-making with belief interval distance," in *Belief Functions: Theory and Applications*. Cham: Springer International Publishing, 2016, pp. 66–74.

[31] D. Han, J. Dezert, and Y. Yang, "Belief interval-based distance measures in the theory of belief functions," *IEEE Transactions on Systems Man Cybernetics-Systems*, vol. 48, no. 6, pp. 833–850, 2018.

[32] Y. Tang, L. Zhang, Q. Teng, F. Min, and A. Song, "Triple cross-domain attention on human activity recognition using wearable sensors," *IEEE Transactions on Emerging Topics in Computational Intelligence*, 2022.

[33] W. Zheng, L. Yan, C. Gou, and F.-Y. Wang, "Meta-learning meets the internet of things: Graph prototypical models for sensor-based human activity recognition," *Information Fusion*, vol. 80, pp. 1–22, 2022.

[34] J. Ding, Y. Wang, H. Si, S. Gao, and J. Xing, "Multimodal fusion-adaboost based activity recognition for smart home on wifi platform," *IEEE Sensors Journal*, vol. 22, no. 5, pp. 4661–4674, 2022.

[35] K. Chen, L. Yao, D. Zhang, X. Wang, X. Chang, and F. Nie, "A semisupervised recurrent convolutional attention model for human activity recognition," *IEEE Transactions on Neural Networks and Learning Systems*, vol. 31, no. 5, pp. 1747–1756, 2020.

[36] W. Gao, L. Zhang, Q. Teng, J. He, and H. Wu, "DanHAR: Dual attention network for multimodal human activity recognition using wearable sensors," *Applied Soft Computing*, vol. 111, pp. 107–125, 2021.

[37] H. F. Nweke, Y. W. Teh, M. A. Al-Garadi, and U. R. Alo, "Deep learning algorithms for human activity recognition using mobile and wearable sensor networks: State of the art and research challenges," *Expert Systems with Applications*, vol. 105, pp. 233–261, 2018.

[38] V. Nair and G. E. Hinton, "Rectified linear units improve restricted boltzmann machines," in *ICML*, 2010.

[39] D. Anguita, A. Ghio, L. Oneto, X. Parra Perez, and J. L. Reyes Ortiz, "A public domain dataset for human activity recognition using smartphones," in *Proceedings of the 21th international European symposium on artificial neural networks, computational intelligence and machine learning*, 2013, pp. 437–442.

[40] R. Chavarriaga, H. Sagha, A. Calatroni, S. T. Digumarti, G. Tröster, J. d. R. Millán, and D. Roggen, "The opportunity challenge: A benchmark database for on-body sensor-based activity recognition," *Pattern Recognition Letters*, vol. 34, no. 15, pp. 2033–2042, 2013.

[41] M. Sokolova and G. Lapalme, "A systematic analysis of performance measures for classification tasks," *Information Processing & Management*, vol. 45, no. 4, pp. 427–437, 2009.

[42] M. Eastwood and C. Jayne, "Evaluation of hyperbox neural network learning for classification," *Neurocomputing*, vol. 133, pp. 249–257, 2014.

[43] A. Wang, G. Chen, J. Yang, S. Zhao, and C.-Y. Chang, "A comparative study on human activity recognition using inertial sensors in a smartphone," *IEEE Sensors Journal*, vol. 16, no. 11, pp. 4566–4578, 2016.

[44] B. Ganapati, T. Nicholas, S. Holly, and U. Y. Ogras, "w-HAR: An activity recognition dataset and framework using low-power wearable devices," *Sensors*, vol. 20, no. 18, pp. 5356–5372, 2020.

[45] Q. Ni, Z. Fan, L. Zhang, C. D. Nugent, I. Cleland, Y. Zhang, and N. Zhou, "Leveraging wearable sensors for human daily activity recognition with stacked denoising autoencoders," *Sensors*, vol. 20, no. 18, pp. 5114–5136, 2020.

[46] Y. Dong, X. Li, J. Dezert, M. Omar Khyam, M. Noor-A-Rahim, and S. S Ge, "Dezert-Smarandache theory-based fusion for human activity recognition in body sensor networks," *IEEE Transactions on Industrial Informatics*, vol. 16, no. 11, pp. 7138–7149, 2020.

[47] N. Y. Hammerla, S. Halloran, and T. Plötz, "Deep, convolutional, and recurrent models for human activity recognition using wearables," *arXiv preprint arXiv:1604.08880*, 2016.

[48] M. Zeng, L. T. Nguyen, B. Yu, O. J. Mengshoel, J. Zhu, P. Wu, and J. Zhang, "Convolutional neural networks for human activity recognition using mobile sensors," in *6th international conference on mobile computing, applications and services*. IEEE, 2014, pp. 197–205.

[49] F. J. Ordóñez and D. Roggen, "Deep convolutional and lstm recurrent neural networks for multimodal wearable activity recognition," *Sensors*, vol. 16, no. 1, p. 115, 2016.

[50] Q. Teng, K. Wang, L. Zhang, and J. He, "The layer-wise training convolutional neural networks using local loss for sensor-based human activity recognition," *IEEE Sensors Journal*, vol. 20, no. 13, pp. 7265–7274, 2020.

[51] D. Han, J. Dezert, and Y. Yang, "Two novel methods for bba approximation based on focal element redundancy," in *2015 18th International Conference on Information Fusion (Fusion)*. IEEE, 2015, pp. 428–434.

[52] R. R. Yager, "On the dempster-shafer framework and new combination rules," *Information Sciences*, vol. 41, no. 2, pp. 93–137, 1987.

[53] C. K. Murphy, "Combining belief functions when evidence conflicts," *Decision Support Systems*, vol. 29, no. 1, pp. 1–9, 2000.

[54] Y. Dong, X. Li, and J. Dezert, "A new probabilistic transformation based on evolutionary algorithm for decision making," in *20th International Conference on Information Fusion (Fusion)*, 2017, pp. 1–8.

Yilin Dong was born in Yancheng, China, in 1990. He received the Ph.D. degree in Control Science and Engineering from the School of Automation, Southeast University, Nanjing, China, in 2020. Afterwards, he joined College of Computer Science and Engineering, Shanghai Maritime University, Shanghai, China. His research interests include belief function theory, information fusion, and pattern recognition.

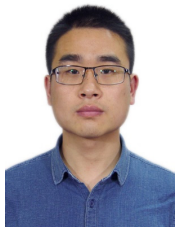

Kezhu Zuo is currently working toward the Ph.D. degree in electronic information from School of Cyber Science and Engineering, Southeast University, Nanjing, China. His research interests include belief function theory, information fusion, and pattern recognition.

Xinde Li (M'09-SM'16) earned his Ph.D. in Control Theory and Control Engineering, from Department of Control Science and Engineering, Huazhong University of Science and Technology (HUST), Wuhan, China, in 2007. Afterwards, he joined School of Automation, Southeast University, Nanjing, China, where he is currently a professor. He was an Academician of Russian Academy of Natural Sciences elected in 2021 and a cover person of Scientific Chinese in the same year, a Fellow of the Institute of Engineering Technology (FIET) in 2022. He was a vice director of Intelligent Robot Committee of Chinese Association for Artificial Intelligence from 2017, a vice director of Intelligent Products and Industry Working Committee of Chinese Association for Artificial Intelligence from 2019. His research interests include Artificial Intelligence, Intelligent Robot, Machine Perception and Understanding, and human-robot interaction, etc. He has undertaken many national key projects, i.e. National 863 key project, NSFC key project, etc. and has published more than 100 high quality papers and 2 books, and owns 26 national invention patents. He also won many prizes, i.e. International Contribution Award, Jiangsu Provincial Science and Technology Award , Scientific and Technological Progress Award in CAA, etc.

Jean Dezert was born in L'Hay les Roses, France, in 1962. He received the Ph.D. degree from the University Paris XI, Orsay, France, in 1990. Since 1993, he has been a Senior Research Scientist with the Information Modeling and Processing Department, ONERA, Palaiseau, France. His current research interests focus on belief function theory, particularly for DSmT, which he has developed with Prof. Smarandache.

Rigui Zhou received his Ph.D. degree in the Department of Computer Science and Technology of Nanjing University of Aeronautics and Astronauts (November, 2007), China. From 2008 to 2010, as a Post Doctoral fellow in the Tsinghua University, China. Currently he is a Professor of College of Information Engineering, Shanghai Maritime University, China. His research interests include quantum image processing, quantum reversible logic and quantum genetic algorithm, et al.

Shuzhi Sam Ge (S'90–M'92-SM'99–F'06) received the B.Sc. degree from the Beijing University of Aeronautics and Astronautics, Beijing, China, in 1986, and the Ph.D. degree from Imperial College of Science, Technology and Medicine, University of London, London, U.K., in 1993. He is currently the Founding Director of the Robotics Institute and the Institute of Intelligent Systems and Information Technology, University of Electronic Science and Technology of China, Chengdu, China. He is also the Founding Director of the Social Robotics Laboratory, Interactive Digital Media Institute, National University of Singapore, Singapore, where he is a Professor with the Department of Electrical and Computer Engineering. He is the Editor-in-Chief of the International Journal of Social Robotics. He has served as an associate editor for a number of flagship journals. He has also served as the Vice-President of Technical Activities from 2009 to 2010, Membership Activities from 2011 to 2012, and the IEEE Control Systems Society.